$Hg_{0.04}Zn_{3.96}Sb_3$: Synthesis, Crystal Structure, Phase Transition, and Thermoelectric Properties

B. L. Pedersen,[†] H. Birkedal,[†] E. Nishibori,[‡] A. Bentien,[†,⊥] M. Sakata,[‡] M. Nygren,[§] P. T. Frederiksen,[⊥] and B. B. Iversen*[,†]

Department of Chemistry and Interdisciplinary Nanoscience Center, University of Aarhus, Langelandsgade 140, DK-8000 Aarhus, Denmark; Department of Applied Physics, Nagoya University, Furo-cho, Chikusa, Nagoya 464-8603, Japan; Department of Inorganic Chemistry, Stockholm University, SE-10691 Stockholm, Sweden; and Grundfos A/S, Poul Due Jensens Vej 7, DK-8850 Bjerringbro, Denmark

Received August 9, 2007. Revised Manuscript Received October 9, 2007

The thermoelectric material Zn_4Sb_3 was mercury doped by introduction of 1 at. % Hg into the synthesis mixture, resulting in $Hg_{0.04}Zn_{3.96}Sb_3$. The doped compound and an undoped reference were characterized by multitemperature short wavelength synchrotron X-ray powder diffraction, SEM/EDX, differential scanning calorimetry (DSC), and physical property measurements. Rietveld refinements suggest that mercury substitution takes place solely on the Zn1 framework site of the disordered room temperature β-phase crystal structure, while the interstitial positions are mercury-free. The refined composition suggests a doping level of 0.6%. The remaining mercury is present as elemental Hg as evidenced by SEM/EDX analysis, the presence of peaks corresponding to crystalline Hg below the Hg freezing temperature, and the presence of a drop in the resistivity at the superconducting transition temperature of Hg. Rietveld refinements of multitemperature synchrotron X-ray powder diffraction data (180 K $< T <$ 290 K, $\Delta T =$ 10 K) reveal a significant change in the α–α'–β phase transition temperatures between undoped and 1% Hg-doped samples. This is corroborated by DSC data that show that the transition enthalpies are very small, about 0.1–0.4 J/g. The largest enthalpy change is observed in the α–α' transition for the undoped sample, whereas the largest transition enthalpy is found in the α'–β transition for the Hg-doped compound. Complete thermoelectric properties have been measured in the temperature range 2–400 K on dense samples prepared by spark plasma sintering. The Hg doping has a very large effect on the transport properties in the ordered α-phase crystal structure but only a minor influence on the properties in the disordered β-phase. The thermoelectric figure of merit, ZT, is found to be ~0.3 for both the undoped and the Hg-doped sample at 300 K.

Introduction

The β-phase of Zn_4Sb_3 has caused excitement in the material science community because it has exceptional thermoelectric properties in the "intermediate" temperature range (200–400 °C) where only few alternatives are known.[1] The thermoelectric figure of merit is $ZT = TS^2/\rho\kappa$, where S is the thermopower, ρ the electrical resistivity, κ the thermal conductivity, and T the absolute temperature. It is the extremely low lattice contribution to the thermal conductivity which gives β-Zn_4Sb_3 a high ZT.[1] The initial report claimed maximum ZT values of about 1.2 for pure Zn_4Sb_3 and even higher values for cadmium-doped samples.[1] However, thermal stability of the samples is a problem, and with repeated thermal cycling even much below the β–γ phase transition at 765 K, the thermoelectric properties degrade and impurity phases appear.[2]

β-Zn_4Sb_3 crystallizes in the hexagonal space group $R\bar{3}c$. The original crystal structure led to disagreement between the calculated (6.07 g/cm^3) and observed (6.39 g/cm^3) mass densities, and the refined stoichiometry was also far from the formal stoichiometry used in the closed ampule synthesis.[3] Recently, the structure was re-examined in our group, and three interstitial Zn sites were discovered (Figure 1).[4] Contrary to the earlier structure, no sites with mixed occupancy were found, and the main Zn lattice site was found to be only partly occupied (~89%). The analogous Cd_4Sb_3 compound was very recently investigated by Zelinska et al.[5] They found that Cd_4Sb_3 crystallizes in the same space group and displays the same main sites as Zn_4Sb_3 but has five interstitial Cd sites, in contrast to the three sites in the Zn compound. As in Zn_4Sb_3, the sites are only partly occupied, with the main site having an occupancy of ~82% and the

* Corresponding author. E-mail: bo@chem.au.dk.
[†] University of Aarhus.
[‡] Nagoya University.
[§] Stockholm University.
[⊥] Grundfos A/S.

(1) (a) Caillat, T.; Fleurial, J.-P.; Borshchevsky, A. *J. Phys. Chem. Solids* **1997**, *58*, 1119. (b) Caillat, T.; Borshchevsky, A.; Fleurial, J.-P. U.S. Patent 6,942,728 B2, 2005.
(2) (a) Zhang, L. T.; Tsutsui, M.; Ike, K.; Yamaguchi, M. *J. Alloys Compd.* **2003**, *358*, 252. (b) Pedersen, B. L.; Birkedal, H.; Nishibori, E.; Iversen, B. B. *ICT Proc.* **2006**, 520–523.
(3) Mayer, H. W.; Mikhail, I.; Schubert, K. *J. Less-Common Met.* **1978**, *59*, 43.
(4) (a) Snyder, G. J.; Christensen, M.; Nishibori, E.; Caillat, T.; Iversen, B. B. *Nat. Mater.* **2004**, *3*, 458. (b) Cargnoni, F.; Nishibori, E.; Rabiller, P.; Bertini, L.; Christensen, M.; Snyder, G. J.; Gatti, C.; Iversen, B. B. *Chem.—Eur. J.* **2004**, *10*, 3861.
(5) Zelinska, O. Y.; Bie, H.; Mar, A. *Chem. Mater.* **2007**, *19*, 1518.

10.1021/cm702247b CCC: $37.00
Published on Web 11/16/2007

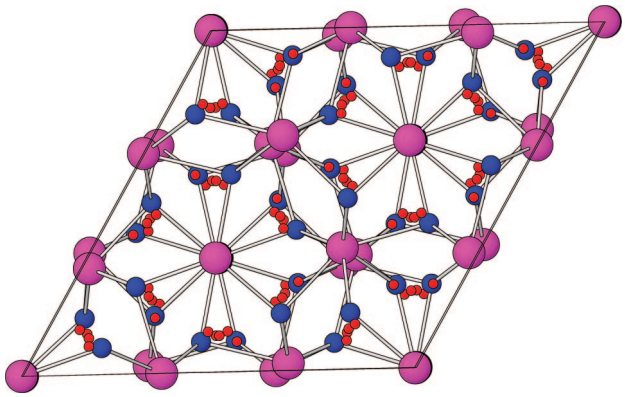

Figure 1. Structure of the β-phase with the three Zn interstitials. Sb is purple, framework Zn is blue, and interstitial Zn is red.

five interstitial sites having occupancies of ~2–7%. The new structure of Zn_4Sb_3 had a correct mass density and a stoichiometry of $Zn_{38.4}Sb_{30}$, and it provided an explanation for why Zn_4Sb_3 behaves like a phonon glass, electron crystal:[6] the interstitial Zn atoms act as very effective phonon scattering centers, leading to the exceptionally low thermal conductivity. Bader topological analysis of the maximum entropy method electron density to a first approximation suggested a Zintl view of the structure with two different types of Sb atoms.[4] The unit cell contains 6 Sb_2^{4-} dimers and 18 Sb^{3-} ions, which together require 39 Zn^{2+} cations for charge balance. The observed p-doping of the systems results from the small deficit of Zn atoms relative to the Zintl stoichiometry. Indeed, band structure calculations show that a material with the ideal stoichiometry will be a narrow band gap semiconductor.[4b]

The Zn_4Sb_3 phase is one of the stable compounds in the Zn–Sb binary system, and it was first reported in 1927 by Takai.[7] The compound Zn_4Sb_3 exists in at least three crystalline phases: the low-temperature α-phase, stable below 263 K; the β-phase, stable from 263 to 765 K; and the high-temperature γ-phase, stable from 765 K until melting at 841 K.[8] Recent work by Mozharivskyj et al. showed the existence of another low-temperature phase based on physical property measurements and evaluation of crystallographic data for both powder and single-crystal samples.[9] When cooling from room temperature, the intermediate phase occurs in the interval 244–218 and 254–234 K for single crystals and polycrystalline samples, respectively. Below these temperatures, the compound transforms into the α-phase. The low-temperature phase was examined by Nylén et al., who found it to be triclinic at 150 K with a complete ordering of the interstitial Zn atoms.[10] Very recently, detailed multitemperature single-crystal investigations by Nylén et al. have unraveled the structure of the intermediate phase, which is now relabeled the α-phase while the lowest temperature phase is the α′-phase.[11] Thus, the nomenclature for the sequence of reversible phase transitions is β–α–α′. The intermediate α-phase is a superstructure of the β-phase, where disordered zinc interstitials and vacancies order into "islands". The subtle transition to the low-temperature α′-phase leads to a modulated structure with further ordering of the partially occupied Zn interstitial positions.[11]

Theoretical calculations on the defect structure revealed by X-ray diffraction predict that slight doping potentially can double the thermopower.[4b] The calculations demonstrated that the Zn interstitials are playing a fundamental role as electron suppliers and Seebeck coefficient enhancers, besides that of lattice thermal conductivity suppressors. However, in order to predict the optimal doping based on theoretical calculations, fundamental knowledge about the crystallographic siting of the dopant element is needed. Many empirical attempts have been made to improve the properties by doping guest atoms into the structure. The initial report of Zn_4Sb_3 thermoelectric properties by Caillat et al. reported an improved thermoelectric performance of a Cd-doped samples with a figure of merit reaching 1.4 at 523 K for $Zn_{3.2}Cd_{0.8}Sb_3$.[1] Record et al. found the solubility of Cd in Zn_4Sb_3 to be ~43 at. %, giving a maximum formal stoichiometry of $Zn_{2.28}Cd_{1.72}Sb_3$,[12] while Nakamoto et al. reported a maximum Cd stoichiometry of $Zn_{2.4}Cd_{1.6}Sb_3$.[13] However, a study by Kuznetsov et al. showed a maximum Cd stoichiometry of only $Zn_{3.76}Cd_{0.24}Sb_3$.[14] Tsutsui et al. found that indium is soluble in Zn_4Sb_3 and produced three single phase $(Zn_{1-x}In_x)_4Sb_3$ samples.[15] The maximum solubility of In was found to be around 3.5 at. %, corresponding to $x = 0.05$, and very small amounts of In doping ($x = 0.005$) improved the thermoelectric figure of merit, whereas ZT degraded for heavily doped samples. This is in agreement with the theoretical calculations of Cargnoni et al., who predicted that slight doping of only 0.33 electron per unit cell would double the thermopower and possibly have dramatic effects on the thermoelectric properties.[4b]

Here we investigate Hg doping of Zn_4Sb_3 by comparing two samples: a pure Zn_4Sb_3 sample and a sample doped with 1 at. % Hg. We use high-resolution, multitemperature synchrotron X-ray powder diffraction data, SEM/EDX, TGA/DSC, and transport measurements to probe the effects of the slight doping on the crystal structure and physical properties.

Experimental Section

Synthesis. The samples were prepared from 99.99% zinc shots, 99.5% antimony powder, and 99.5% liquid mercury. The elements were weighed in stoichiometric ratios in a quartz ampule, which was evacuated and sealed. After sealing, the ampule was placed horizontally in a furnace and heated with a 400 K/h ramp to 973 K

(6) Slack, G. A. In *New Materials and Performance Limits for Thermoelectric Cooling*; Rowe, D. M., Ed.; CRC Press: Boca Raton, FL, 1995.
(7) Takai, T. *Sci. Rep. Tohoku* **1927**, *16*, 1031.
(8) Mosharivskyj, Y.; Pecharsky, A. O.; Bud'ko, S.; Miller, G. J. *Chem. Mater.* **2004**, *16*, 1580.
(9) Mozharivskyj, Y.; Janssen, Y.; Harringa, J. L.; Kracher, A.; Tsokol, O. A.; Miller, G. J. *Chem. Mater.* **2006**, *18*, 822.
(10) (a) Nylén, J.; Andersson, M.; Lidin, S.; Häussermann, U. *J. Am. Chem. Soc.* **2004**, *126*, 16306. (b) Mikhailushkin, A. S.; Nylén, J.; Häussermann, U. *Chem.—Eur. J.* **2005**, *11*, 4912.
(11) Nylen, J.; Lidin, S.; Andersson, M.; Iversen, B. B.; Lie, H.; Newman, N.; Hausserman, U. *Chem. Mater.* **2007**, *19*, 834.
(12) Record, M. C.; Izard, V.; Bulanova, M.; Tedenac, J. C. *Intermetallics* **2003**, *11*, 1189.
(13) Nakamoto, G.; Souma, T.; Yamaba, M.; Kurisu, M. *J. Alloys Compd.* **2004**, *377*, 59.
(14) Kuznetsov, V. L.; Rowe, D. M. *J. Alloys. Compd.* **2004**, *372*, 103.
(15) Tsutsui, M.; Zhang, L. T.; Ito, K.; Yamaguchi, A. *Intermetallics* **2004**, *12*, 809.

under continuous rotation. The sample was held at this temperature for 2 h before quenching in ice–water. This resulted in a polycrystalline solid, which was ground in an agate mortar to give a homogeneous powder.

Warning: elemental mercury has a high vapor pressure and is toxic. Protective clothing should be used, and the mixing should be done in a fumehood.

To ensure that the sample was single phase, a powder diffraction pattern was recorded using Cu Kα radiation in a 2θ range of 8–84° with a Stoe STADI P diffractometer at the Department of Chemistry, University of Aarhus.

Synchrotron Powder Diffraction. A homogeneous grain size is important for measuring high-quality powder diffraction data. Thus, the samples were sieved (45 μm), and only the smaller crystallites were used. The powders were then floated with ethyl alcohol in a Petri dish and left for sedimentation. After 1 min, the top layer of the ethyl alcohol was removed into a new Petri dish and left for further sedimentation for 5 min. The top layer was again removed into a new Petri dish, and the ethyl alcohol was evaporated, leaving a sample fraction of homogeneous grain size. The samples were transferred to 0.2 mm capillaries and held in an ultrasound bath for about 5 min to obtain a dense packing of the powders.

Long exposure data sets (70 min) were recorded at $\lambda = 0.420\,998$ Å at 300 and 180 K. Multitemperature diffraction data in the range of 190–290 K, $\Delta T = 10$ K, were recorded with 7 min exposure time ($\lambda = 0.420\,998$ Å). All data sets were Rietveld refined with the program FULLPROF[16] using a pseudo-Voigt profile function and a background modeled with linear interpolation between ~65 points. A second impurity phase ZnSb (4.5% for the Hg sample, 16.5% for the pure sample) was included in the refinements. For the α-phase refinements it was necessary to restrict the data set to $2\theta < 35°$ because the maximal number of reflections allowed in Fullprof was exceeded due to the complex structure. Two series of refinements were carried out on the multitemperature data: one refining the α-phase moving up in temperature and one refining the β-phase moving down in temperature. The structure of Nylén et al.[10] was used for refining the α/α′-phase. Since it is a very complex structure with 46 atomic sites, only background, zero point, lattice, and profile parameters could be refined. Atomic displacement parameters (ADPs) at a given temperature were estimated by linear extrapolation from the results of the multitemperature β-phase refinements.

Thermal Analysis. Differential scanning calorimetry (DSC) was performed on a Netzsch STA 449 C using Al crucibles with pierced lids and a heating/cooling rate of 10 K/min. The experiments were performed in a He atmosphere using gaseous nitrogen for cooling rather than liquid nitrogen since this resulted in more stable conditions and facilitated the measurements of the very weak DSC signals associated with the phase transitions.

Microstructure. The microstructure was examined on pressed pellets of the Hg-doped sample using SEM/EDX. The sample was pressed using spark plasma sintering (SPS), where the powder sample was loaded into a graphite die and hot-pressed under argon at 673 K for 180 s with a pressure of 100 MPa. This resulted in a crack-free sample with a relative density greater than 99%. The sample was cut with a diamond saw and polished using progressively finer silicon carbide paper ending with 4000 mesh. For SEM/EDX a CamScan Maxim microscope was used with 20 kV acceleration voltage. The emitted X-rays were detected with a liquid N_2 cooled solid-state detector; K, L, and M lines were detected for Zn, Sb, and Hg, respectively.

(16) Rodríguez-Carvajal, J. Fullprof2000, 2001.

Transport Properties. Measurements of transport properties were done on pellets compacted by SPS. Both samples had a density of more than 99% of the theoretical density as measured on a home-built device based on Archimedes' principle. The physical properties are highly dependent on the sample preparation, and a low sample density or macroscopic cracks will lead to poor performance. Indeed, Pedersen et al. have shown that a change in sample density from 90% to 100% can triple the thermoelectric figure of merit for Zn_4Sb_3 samples.[17] The thermal transport option (TTO) of a Quantum Design PPMS was used to measure the Seebeck coefficient, thermal conductivity, and resistivity using a four-probe lead configuration and silver-filled epoxy glue contacts.

Results and Discussion

Dopant Atom Siting. A large effort was made to locate the dopant atom position from the high-resolution synchrotron powder diffraction data using Rietveld refinements. A number of different refinement strategies have been tested, in the attempt to find the dopant atom location. Initially, the long exposure 300 K data set was refined with the model containing three interstitial Zn sites. In the refinements of Cargnoni et al., the occupancies of Zn2 and Zn3 were constrained to be identical. In order not to bias the subsequent dopant atom refinement, this constraint was removed in refinement of the Hg-doped sample. The initial refinement gave a stoichiometry of $Zn_{38.12(7)}Sb_{30}$, which corresponds to a slightly lower Zn content than the Cargnoni et al. refinement ($Zn_{38.4}Sb_{30}$). It is conceivable that different samples have slightly varying Zn occupancies and that this is a major contributor to the very large variation in thermoelectric properties reported for Zn_4Sb_3 samples in the literature.[17]

In the subsequent refinement, an Hg atom was introduced at each of the Zn sites. The occupancy of the Hg atom was subtracted from the refined occupancy of the Zn atom at the same position, thus fixing the sum of Hg and Zn to be equal to the Zn occupancy of the initial refinement. This was done separately for each of the four Zn sites, but in none of the cases was a stable, converging refinement achieved. In the next approach the occupancy constraint was removed, and the occupancies of both Zn and Hg were refined independently. Like in the previous model, Hg was introduced on each of the four Zn sites in turn so that after four cycles all four Zn sites had a potential Hg substitution. To avoid effects originating from the chosen starting point in parameter space, we performed the refinement series four times in each case starting with Hg substitution on a different Zn site. In all cases, a stable converging refinement was reached, but only the Zn1 framework site indicated the presence of Hg substituting for Zn, since the refined occupancy revealed a small but positive value. The three interstitial Zn sites all refined to a negative Hg occupancy value, thereby strongly indicating that no Hg is present on these sites. Refinements of the Hg occupancy on the Zn1 site suggested a total composition of $Zn_{37.60(14)}Hg_{0.22(4)}Sb_{30}$, which means that 0.58(10)% Hg is incorporated into the structure. Since the sample was prepared to contain 1% Hg in a closed ampule,

(17) Pedersen, B. L.; Birkedal, H.; Iversen, B. B.; Nygren, M.; Frederiksen, P. T. *Appl. Phys. Lett.* **2006**, *89*, 242108.

the remaining 0.4% is likely to be present as inclusions of elemental Hg, which has a melting point of 234.32 K. Thus, it would be on liquid form in the data recorded at 300 K and not detectable by diffraction.

To further support the siting of the Hg dopants, theoretical model based tests were made to determine whether the signal-to-noise ratio in the data was good enough to actually allow detecting 1% Hg substitutions. This was done by calculating the difference between the Hg-free model obtained from refinement against the Hg data and a model where 1% Hg was placed on one of the four Zn sites. In each of the four cases, comparison with the standard uncertainty of the measured data clearly shows that the changes due to Hg substitution are significant and different for each site (Figure S1, Supporting Information). The refinement residuals of each model is given in Table ST1, Supporting Information. This confirms that the data are of sufficient quality to conclusively determine the Hg siting.

The presence of residual Hg should become visible in the data below the melting point of Hg. However, this temperature coincides with the $\beta \rightarrow \alpha$ phase transition of Zn_4Sb_3 which induces a wealth of new diffraction peaks, making it challenging to conclusively locate additional lines specific to solid mercury. Nevertheless, new lines consistent with solid Hg do appear (Figure S2, Supporting Information). Below we show that there indeed is elemental Hg present as inclusions in the samples, which strongly support the X-ray diffraction results.

We then considered the 180 K data set. As previously mentioned, Nylén et al. proposed a triclinic α-phase structure with complete ordering of the Zn atoms.[10] This structure has 26 individual Zn sites, where 21 sites originate from the Zn1 framework site in the β-phase and the remaining 5 Zn sites from the 3 interstitial Zn sites. With only 0.58(10)% Hg incorporated in the structure, it is very challenging to locate the dopant atom sites after the $\beta \rightarrow \alpha$ phase transformation. Because of the highly complex structure, the ADP's were estimated from the β-phase values by linear extrapolation and constrained to be identical for all Zn atoms. The same was done for Sb atoms. Introducing Hg on each Zn site, one by one, led to a stable refinement where 9 Zn sites of the triclinic α-phase structure indicated the presence of Hg. This is consistent with the result from the β-phase, but the amounts are too small to be statistically significant, so it should be stressed that the result are indicative. The refinements indicated a stoichiometry of $Zn_{51.28(6)}Hg_{0.20(2)}Sb_{40}$ for the α-phase, corresponding to 0.40(5)% Hg substitution, which is slightly lower than estimated for the β-phase. Metallic Hg was also introduced in the refinements leading to a reduction in the refinement R factors. The refinements suggested 0.71(1)% metallic mercury in the sample at low temperatures. Since it is not possible to estimate the amount of metallic Hg at room temperature by diffraction, it is impossible to determine whether some of the mercury is being excluded when the structure transforms from the $\beta \rightarrow \alpha$ phase.

As described in the Experimental Section, multitemperature data with short exposure (7 min) as well as long exposure (70 min) data at 180 and 300 K were collected. The long exposure data provide very high signal-to-noise ratio and better allow detection of small impurity phases. The Rietveld refinement results for the short exposure data are entirely consistent with the results from the long exposures. In the β-phase refinements of the 7 min data at 290 K, indication of Hg presence is also exclusively found at the Zn1 site, but the refined Hg occupancy suggests a slightly lower content (0.40(5)%). In the α-phase refinements of the 7 min 190 K data, Hg is detected on five out of the nine sites found in the long exposure 180 K data, and the total amount is 0.24%. The five sites correspond to the highest occupancy sites of the long exposure refinements.

Table 1. Crystallographic Details from Rietveld Refinement of Pure and 1% Hg-Doped Zn_4Sb_3 at 290 K

	Zn_4Sb_3	$Hg_{0.04}Zn_{3.96}Sb_3$
exposure time (min)	7	7
no. of data points	7516	7517
no. of reflections	4923	4872
no. of parameters	78	88
R_F (%)	1.42	1.35
R_{Bragg} (%)	2.87	1.83
R_p (%)	3.25	2.96
R_{wp} (%)	4.53	4.31
X^2	10.9	9.68
$a = b$ (Å)	12.22577(8)	12.23367(12)
c (Å)	12.41521(10)	12.42790(13)
X	0.263(5)	0.200(3)
Y	0.0150(5)	0.0123(3)
Biso Sb1	1.21(3)	1.10(2)
Biso Sb2	1.05(3)	1.01(3)
Biso Zn	1.79(5)	1.84(5)
occupancy Zn1	0.903(3)	0.909(3)
occupancy Zn2	0.060(1)	0.047(1)
occupancy Zn3	0.060(1)	0.058(2)
occupancy Zn4	0.057(2)	0.040(1)
volume ($Å^3$)	1607.08(2)	1610.80(3)

Table 2. Atomic Positions of Pure and 1% Hg-Doped Zn_4Sb_3 Derived from Rietveld Refinement of 290 K Data Set

site	x	y	z
Sb1 Hg	0.3561(1)	0.0000 (0)	0.2500 (0)
Sb1 pure	0.3556(1)	0.0000 (0)	0.2500 (0)
Sb2 Hg	0.0000(0)	0. 0000(0)	0.1365(1)
Sb2 pure	0.0000(0)	0.0000(0)	0.1362(1)
Zn1 Hg	0.0789(1)	0.2442(1)	0.4028(1)
Zn1 pure	0.0786(1)	0.2445(1)	0.4047(1)
Zn2 Hg	0.1636(20)	0.4218(21)	0.0599(23)
Zn2 pure	0.1561(19)	0.4238(19)	0.0521(19)
Zn3 Hg	0.2478(19)	0.4537(19)	0.1873(22)
Zn3 pure	0.2515(21)	0.4278(24)	0.1855(24)
Zn4 Hg	0.1140(30)	0.2265(26)	0.2762(22)
Zn4 pure	0.1008(22)	0.2185(21)	0.2833(17)

Multitemperature Data. To study the effect of the inclusion of Hg in the crystal structure, multitemperature synchrotron powder diffraction data are used to examine the α′–α–β phase transitions. Full crystallographic data and refinement details are given for the 290 K data set of both pure and Hg-doped samples in Tables 1 and 2. Crystallographic data and details of the remaining α- and β-phase multitemperature synchrotron powder diffraction refinements are given in Tables ST1–ST4 of the Supporting Information for both the pure and the Hg-doped samples. Observed and calculated diffraction patterns for the α-phase (190 K) and the β-phase (290 K) are shown in Figures 2 and 3.

Figure 4 shows the integral breadth, β, defined as $\beta = A/I_0$, where A is the area of the rectangle having the same width and height as the line profile and I_0 is the maximum

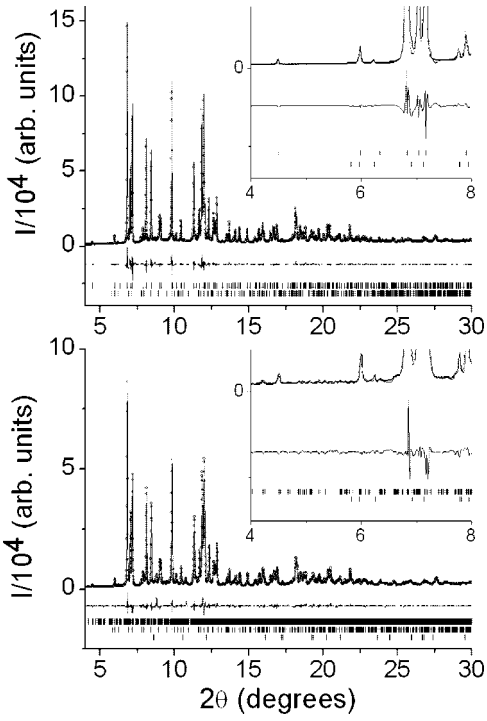

Figure 2. Observed (circle), calculated (line), and difference synchrotron X-ray diffraction patterns for $Hg_{0.04}Zn_{3.96}Sb_3$ for the β-phase (top, 290 K) and the α-phase (bottom, 190 K). The vertical lines indicate the position of Bragg peaks for the Zn_4Sb_3 (top) and ZnSb (bottom) phases in the β-phase and Zn_4Sb_3 (top), ZnSb (middle), and metallic mercury (bottom) in the α-phase. Insets show a blowup of the low-order region.

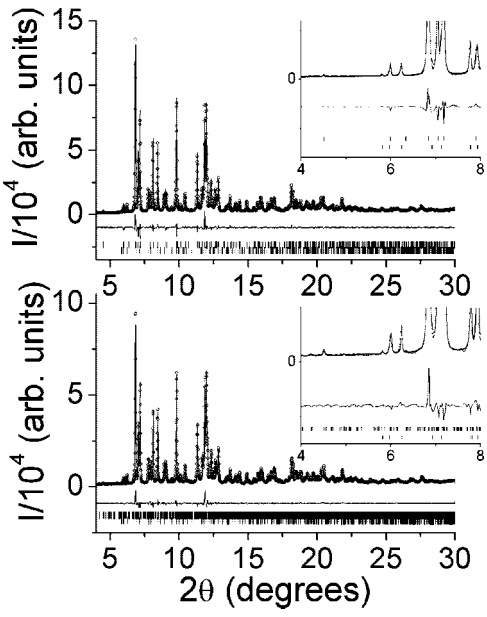

Figure 3. Observed (circle), calculated (line), and difference synchrotron X-ray diffraction patterns for pure Zn_4Sb_3 for the β-phase (top, 290 K) and the α-phase (bottom, 190 K). The vertical lines indicate the position of Bragg peaks for the Zn_4Sb_3 (top) and ZnSb (bottom) phases. Insets show a blowup of the low-order region.

intensity of the line profile. Although a phase transition normally can be detected by peak-splitting and appearance of additional peaks, the complex structure of Zn_4Sb_3 gives rise to approximately 5000 and 13 000 peaks within our data range in the β- and α-phases, respectively. This means that the α-phase peaks are very close to the 2θ position of the β-phase peaks, and an effective peak broadening is observed

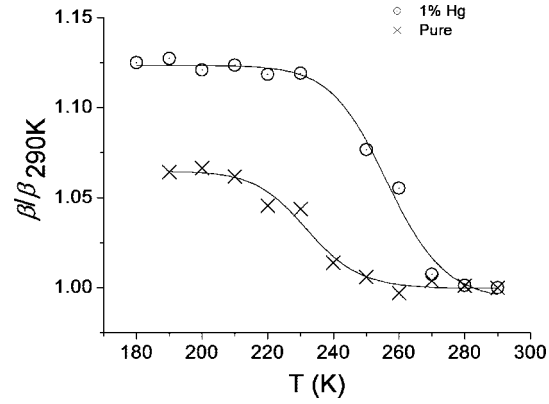

Figure 4. Normalized integral breadth as a function of temperature for undoped Zn_4Sb_3 (crosses) and 1% Hg-doped Zn_4Sb_3 (circles).

instead of peak splitting. The detailed crystal structure used in the α-phase refinements is given in Table ST5 of the Supporting Information. We have modeled the multitemperature data sets, using a pseudo-Voigt function and subsequently calculated the integral breadth normalized to the 290 K data set. The trend has been modeled by a sigmoidal function.

Both data series display a sudden change in normalized integral breadth when moving from RT toward lower temperatures. In the case of the pure sample, the increase begins at ~250 K and ends around 220 K, indicating that the phase transition is taking place in this temperature interval. This is consistent with the phase transition temperature of 254 K for polycrystalline samples reported by Mozharivskyj et al.[9] For the mercury-doped sample, the increase has shifted, starting at 270–280 K and ending at 230 K, indicating that the phase transition is taking place over a larger temperature span. The temperature resolution of the experiment (10 K) does not permit detecting the presence of two distinct phase transitions, $\beta \rightarrow \alpha$ and $\alpha \rightarrow \alpha'$. It is noteworthy that metallic mercury was detected in all refinements from 190 to 230 K. The refinements consistently suggested ~0.71(1)% solid mercury. In the 240 K data set, metallic Hg was still present, but the amount had decreased to ~0.2%. In the 250 K data set, no metallic Hg could be detected. As previously mentioned, the melting point for mercury is 234.32 K, which is consistent with the disappearance of the solid mercury lines in the powder pattern.

Microstructure and Hg Inclusion. The microstructure of the sample was investigated by SEM/EDX. Figure 5 shows elemental maps determined by EDX recorded at the Hg (M-edge), Sb (L-edge), and Zn (K-edge) as well as a line scan across the sample. The maps clearly show the presence of Hg inclusions as spots of high Hg content coinciding with low Sb and Zn content. There are also sites, one of which is indicated by the white arrow in Figure 5A, of low Sb and Hg content, but high Zn content, possibly caused by a small Zn exclusion. This is consistent with Zn evaporating from the structure or with the presence of the ZnSb impurity. In the line scan the concentration of Hg increases from ~5 to ~20 μm, and the concentration of both Sb and Zn decreases in the same region. This is consistent with the presence of Hg inclusions. Sb experiences a small decrease in the 30–40

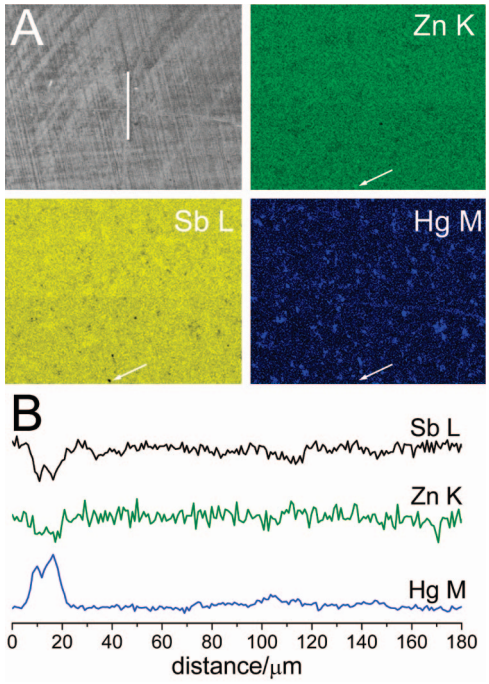

Figure 5. (A) SEM image of the $Zn_{3.96}Hg_{0.04}Sb_3$ sample and elemental maps of Hg (M-edge), Sb (L-edge), and Zn (K-edge). The white line is 180 μm and indicates where the line scan shown in (B) was recorded. (B) Sb, Zn, and Hg EDX spectra observed in a line scan of $Zn_{3.96}Hg_{0.04}Sb_3$.

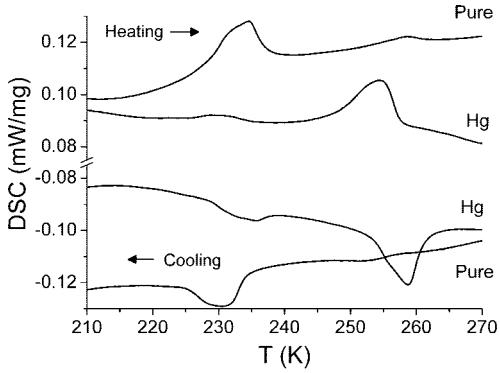

Figure 6. DSC of Zn_4Sb_3 and $Zn_{3.96}Hg_{0.04}Sb_3$ during cooling and heating.

μm region, where the Hg concentration is stable and no clear effect is seen in the Zn concentration (due to noisy signal), consistent with the presence of small Zn exclusions or the ZnSb impurity. The Sb content also decreases around 100–120 μm and 140–150 μm, and at both times there is a small increase in Hg concentration indicating Hg inclusions.

Thermal Analysis. Figure 6 shows the DSC signal recorded by cooling and heating of the mercury-doped sample and the pure reference sample synthesized by the exact same procedures. The signatures of the phase transitions are very weak but still measurable and fully reproducible. Upon cooling, the signal for the pure Zn_4Sb_3 sample displays a minor peak with an onset temperature of 259.0 K and a large peak with onset temperature at 233.0 K. This is consistent with the second-order β–α phase transition at 254 K and the first-order α–α' phase transition at 234 K reported by Mozharivskyj et al.[9] Heating of the same sample shifts the α'–α phase transition temperature to a slightly lower value (230.7 K), which can be expected due to hysteresis around a first-order phase transition. The α'–β phase transition occurs at 252.3 K, which is somewhat in disagreement with the observations of Mozharivskyj et al.,[9] who did not detect hysteresis for this transition.

The Hg-doped sample also displays two peaks in the DSC signal, but the signal size is switched so that the onset temperature of the major peak occurs at 257.7 K on cooling, corresponding to the β–α phase transition, and the onset temperature of the minor peak occurs at 232.2 K, corresponding to the α–α' phase transition. When heating the sample, the onset of the major peak is at 253.2 K and the onset of the minor peak is at 229 K. Although the presence of Hg inclusions in the sample has been confirmed by EDX, these cannot account for the difference relative to the pure sample. The melting point for mercury is 234 K, so any signal from Hg inclusions should be coinciding with the α–α' phase transition, which is the weak signal for the doped sample. Hence, freezing of Hg is unlikely to be the explanation for the observed change in peak areas. We note that we have also measured elemental Hg freezing/melting traces. In these data, the melting temperature is 232.8 K while freezing is 228.1 K. The major peak for the Hg-doped Zn_4Sb_3 sample is on both cooling and heating at a higher temperature. The phenomenon therefore has to be of intrinsic character and caused by Hg substitution on the Zn1 site. To support this, the possible contribution from elemental Hg has been estimated using the melting enthalpy (11.44 J/g) of pure elemental Hg. If we assume that none of the Hg is sited in the structure, a contribution of 0.15 J/g should be expected, corresponding to 1.27 wt % Hg in the sample (= 1 at. %). The measured enthalpy change at the phase transition upon heating is only 0.10 J/g, which means some of the Hg must be incorporated in the structure. Since ordering of the interstitial atoms is the key factor in the phase transitions,[17] even minute doping of 0.6% Hg has a substantial effect on the system. If the changes in the crystal structures with temperature are the same for the Hg-doped system as for the undoped system, it is interesting to observe that the presence of Hg on the main framework site makes the ordering of the Zn interstitials and vacancies much more unfavorable. However, detailed multitemperature single crystal investigations are needed to further clarify the detailed structural origin of the phase transitions in the Hg-doped system.

Thermoelectric Properties. The mercury doping has very significant effects on the thermoelectric properties of Zn_4Sb_3. In Figure 7 the thermopower is shown for both samples between 2 and 400 K. In the ordered α/α'-phase, the Seebeck coefficient for the Hg-doped sample is around twice as large as for the undoped sample, but at the α–β phase transition the value decreases dramatically and reaches the same level as for pure Zn_4Sb_3. The phase transition can be detected in the thermopower in both samples but is extremely pronounced in the Hg-doped sample. In correspondence with the PXRD data the β–α phase transition occurs ~10 K higher for the doped sample (270 K) compared with the undoped sample (260 K). For the doped sample both phase transitions are reflected in the thermopower (α–α' at 230 K), while the pure sample has one broad signature.

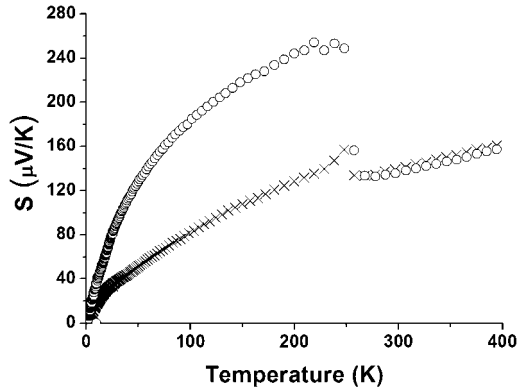

Figure 7. Thermopower of undoped Zn_4Sb_3 (crosses) and $Zn_{3.96}Hg_{0.04}Sb_3$ (circles).

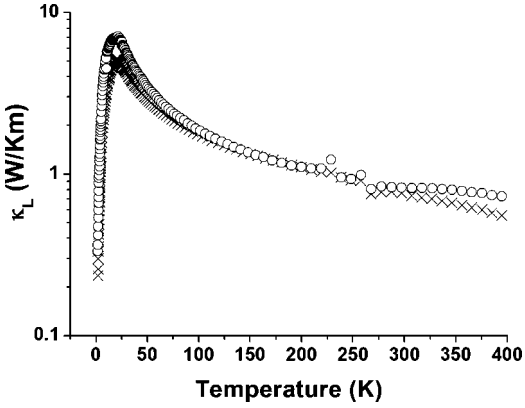

Figure 8. Thermal conductivity of undoped Zn_4Sb_3 (crosses) and $Zn_{3.96}Hg_{0.04}Sb_3$ (circles).

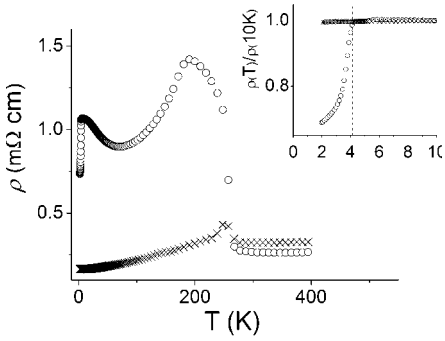

Figure 9. Resistivity of undoped Zn_4Sb_3 (crosses) and $Zn_{3.96}Hg_{0.04}Sb_3$ (circles).

Figure 8 shows the lattice contribution to the thermal conductivity. Here both samples display the same trend, and approximately the same value, although there might be a tendency to higher thermal conductivity for the 1% Hg sample above the phase transition. This may, however, be an unphysical result because PPMS measurements of thermal conductivity are known to become less reliable above room temperature. In the κ_L data the two phase transitions occur approximately at the same temperature, 270 and 230 K, but as for the Seebeck coefficient the transitions are more clearly seen in the doped sample.

The electrical resistivity is shown in Figure 9. It is clear that the doping has a large effect on the resistivity in the α-phase. Just before the phase transition, the value for

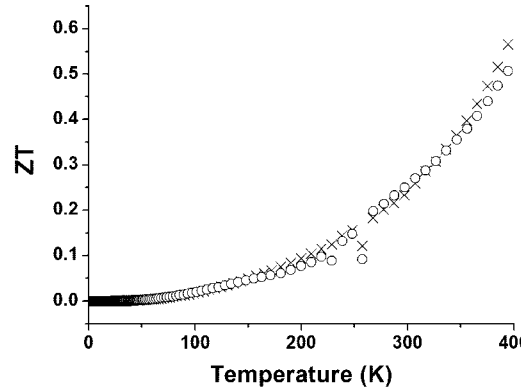

Figure 10. Figure of merit of undoped Zn_4Sb_3 (crosses) and $Zn_{3.96}Hg_{0.04}Sb_3$ (circles).

the Hg-doped sample is almost 4 times higher than for the undoped sample, but after the phase transition it is slightly lower. In a simple picture this may be rationalized as if the Hg atoms mainly act as electron donors in the defect structure, which they apparently do better than Zn. In the α-phase they are incorporated into the ordered crystal lattice, and here the uneven chemical bonds formed between Hg and Zn and the rest of the framework leads to an increased resistivity. More detailed analysis would require complete single crystal structural characterization of the phase transition coupled with measurements of charge carrier concentrations. Around 4 K, the resistivity decreases in the doped sample. This coincides with the critical temperature of superconductivity for solid Hg (4.15 K), and it is consistent with the observation of excess Hg being present as inclusions.

The physical properties are summed up by the thermoelectric figure of merit, which can be seen in Figure 10. Although doping has a large effect on individual physical properties such as the Seebeck coefficient and the resistivity, the effects are largely canceling out. Thus, the figure of merit is almost identical for the two samples. This could lead to speculations, whether ZT actually could be improved if all of the added mercury was incorporated into the structure. There is a slight tendency that the doped sample has a higher ZT at elevated temperatures, but it is difficult to perform a reliable extrapolation. On the other hand, cation doping may be beneficial for stabilizing the β-phase at higher temperatures to make the material applicable in thermoelectrical applications. The high-temperature properties of the doped sample are currently under investigation.

Conclusions

Synchrotron powder diffraction has been used in the attempt to locate the dopant atom siting in a 1% Hg-doped Zn_4Sb_3 sample. Rietveld refinement of the data suggests a mercury doping level of 0.58(10)%, all located at the Zn1 framework site. The remaining Hg is found as elemental Hg inclusions by SEM/EDX. The slight Hg doping has a large effect on both the physical properties and on the structural phase transitions in the system. Peak width analysis reveals that the β–α phase transition occurs ~10 K higher in temperature in the doped sample (270 K), which is corroborated by the thermopower data. Overall, the doping has

a very large effect on the thermopower and the resisitivity in the low-temperature α-phase, whereas the β-phase values are comparable. The doping only has small effect on the lattice contribution to the thermal conductivity. A large change in DSC signal is observed for the doped sample relative to the undoped sample. For the undoped sample the α–α′ transition has the major enthalpy change, whereas it is the α–β transition for the Hg-doped sample. Both samples exhibit excellent thermoelectric properties in the β-phase with ZT reaching about 0.3 at 300 K.

Acknowledgment. The authors gratefully acknowledge the beam time obtained at beamline B2BL02 at SPring8, Japan. The work was supported by DANSYNC. H.B. gratefully acknowledges support from the Danish Research Councils.

Supporting Information Available: Model-based calculation of signal-to-noise ratio compared to expected signal from Hg-containing structure visualized in Figure S1; refinement residuals of each model-based calculation (Table ST1); powder pattern of low-temperature $Hg_{0.04}Zn_{3.96}Sb_3$ including Bragg reflections from solid mercury (Figure S2); selected crystallographic details from α- and β-phase refinements of both the pure and the Hg-doped samples (Tables ST2–ST5); detailed crystal structure data including atomic positions of the α-phase (Table ST6). This material is available free of charge via the Internet at http://pubs.acs.org.

CM702247B